

RESEARCH ARTICLE | SEPTEMBER 08 1995

## Nonperturbative approach to femtosecond spectroscopy: General theory and application to multidimensional nonadiabatic photoisomerization processes

Luis Seidner; Gerhard Stock; Wolfgang Domcke




*J. Chem. Phys.* 103, 3998–4011 (1995)


<https://doi.org/10.1063/1.469586>




CrossMark



Lock-in Amplifier



Boxcar Averager



Zurich  
Instruments

Find out more

Boost Your Optics and  
Photonics Measurements

# Nonperturbative approach to femtosecond spectroscopy: General theory and application to multidimensional nonadiabatic photoisomerization processes

Luis Seidner, Gerhard Stock, and Wolfgang Domcke

*Institute of Physical and Theoretical Chemistry, Technical University of Munich, D-85748 Garching, Germany*

(Received 25 April 1995; accepted 2 June 1995)

A general nonperturbative approach to calculate femtosecond pump-probe (PP) signals is proposed, which treats both the intramolecular couplings and the field-matter interaction (numerically) exactly. Experimentally as well as in a perturbative calculation it is straightforward to distinguish between different spectroscopic processes through the direction of the wave vector of the emitted radiation. A nonperturbative calculation, on the other hand, yields the *overall* polarization of the system, which is the sum of all these contributions. We present a general and practical method that allows to extract the individual spectroscopic signals, which are resolved in time, frequency, and direction of the emission, from the overall polarization. We briefly derive the basic expressions for the time- and frequency-resolved PP signals under consideration, and discuss in detail the simplifications that arise when the usual assumptions (i.e., weak laser fields, nonoverlapping pulses, slowly-varying envelope assumption and rotating-wave approximation) are invoked. The computational procedure is illustrated by nonperturbative calculations of the polarizations and PP signals for a one-dimensional shifted harmonic oscillator. To demonstrate the capability of the approach we have evaluated the polarization as well as PP signals for a three-dimensional model system with vibronically coupled potential-energy surfaces, which describes ultrafast nonadiabatic isomerization dynamics triggered by the twisting of a double bond. We consider various wavelengths and pulse durations of the laser fields and study integral and dispersed PP spectra as well as coherent photon-echo signals. It is shown that the time- and frequency-resolved PP signals reflect in real time the disappearance of the reactants and the delayed appearance of the products. © 1995 American Institute of Physics.

## I. INTRODUCTION

The advent of femtosecond optical laser pulses has prompted a rapidly increasing amount of experimental and theoretical work considering the time-resolved spectroscopic investigation of ultrafast molecular dynamics.<sup>1,2</sup> Femtosecond pump-probe (PP) techniques have been applied to monitor in real time the nuclear motion of isolated molecular systems, to study coherent transients in semiconductors and the relaxation dynamics of dye molecules in solution, and to investigate ultrafast processes in biological systems. All these experiments share the idea that the pump pulse prepares a nonstationary state, which is interrogated by the time-delayed probe pulse. Depending on the specific application, the probing of the excited state dynamics is achieved by excited-state absorption with detection of fluorescence or photoproducts,<sup>3</sup> pulsed ionization with ion or photoelectron detection,<sup>4,5</sup> and frequency-integrated,<sup>6</sup> dispersed,<sup>7</sup> or polarization-sensitive<sup>8</sup> detection of the probe-induced emission field.

In the theoretical description of these experiments the time-dependent response of the material system, i.e., the ultrafast dynamics to be observed, enters through the laser-induced nonlinear polarization  $\mathbf{P}(t)$ , which has to be evaluated for appropriate model systems. Most of the theoretical work has employed a perturbative description for the interaction of the molecular system with the laser field.<sup>9–16</sup> More recently, also nonperturbative descriptions have been considered.<sup>17–23</sup> Assuming, as usual, an optically thin

sample, the only formal difference between the two formulations is whether the electric polarization  $\mathbf{P}(t)$  is evaluated in a perturbative or nonperturbative manner.<sup>15,16</sup> As a consequence, the definitions of time- and frequency-resolved PP signals are completely equivalent in both formulations. A perturbative approach is particularly advantageous in cases where the nonlinear system response functions (the multiple time integration of which gives  $\mathbf{P}(t)$ ) can be evaluated analytically, i.e., for few-level systems<sup>9</sup> and the harmonic oscillator.<sup>11,13</sup> In cases where the description of the molecular dynamics requires a numerical wave-packet propagation, on the other hand, the exact treatment of the field-matter interaction requires no major additional effort and is often more straightforward than the cumbersome numerical evaluation of multitime system response functions. Furthermore, the nonperturbative approach allows the investigation of the effects of strong laser fields.<sup>19,22</sup> Besides the obvious point that one needs to propagate the wave function with a time-dependent Hamiltonian instead of a time-independent one, the calculation of PP signals appears to be rather similar in both formulations.

The nonperturbative calculation of PP spectra, however, involves an additional, albeit only technical, problem. Experimentally as well as in a perturbative calculation, it is straightforward to distinguish between different spectroscopic processes via the direction of the wave vector  $\mathbf{k}$  of the emitted radiation. Assuming that the pump and probe fields propagate with the wave vectors  $\mathbf{k}_1$  and  $\mathbf{k}_2$ , respectively, the

direction  $\mathbf{k}$  of a specific laser-induced emission is in general given by a linear combination of  $\mathbf{k}_1$  and  $\mathbf{k}_2$ . For example, the coherent emission due to the photon-echo effect is observed in the directions  $2\mathbf{k}_2 - \mathbf{k}_1$  and  $2\mathbf{k}_1 - \mathbf{k}_2$ , while the transmittance of the pump and probe pulses due to stimulated emission and resonance Raman processes is observed in the  $\mathbf{k}_1$  and  $\mathbf{k}_2$  directions, respectively.<sup>24</sup> In a nonperturbative calculation, however, we obtain the *overall* polarization of the system, which is given as sum of all these processes. Furthermore, for the sake of simplicity one usually assumes a coherent classical electric field. The pump and probe fields thus possess a fixed relative phase, giving rise to a number of additional contributions to the polarization,<sup>25</sup> which are not observed in standard PP experiments, where the signal is incoherently averaged over many laser shots. Thus, although we know that in the weak-field limit the overall polarization reduces to the results from lowest-order perturbation theory, we still have to distinguish the different contributions to  $\mathbf{P}(t)$  in order to calculate a specific experimental PP signal. In existing nonperturbative PP calculations this problem has been circumvented by (i) considering fragmentation cross sections (ions or dissociation fragments) instead of photon detection,<sup>17–19</sup> (ii) considering the time evolution of the system (following pulsed excitation) instead of PP signals,<sup>20,22</sup> or (iii) assuming a strongly repulsive excited potential-energy (PE) surface, and restricting oneself to the time-dependent dynamics in the electronic ground state.<sup>23</sup>

In this work we propose a general approach to calculate nonlinear polarizations and the corresponding PP spectra in a nonperturbative manner. To clarify the approximations involved and to make contact with previous work, we briefly derive the expressions for the PP signals under consideration. We present a general and practical method to extract the individual contributions and spectroscopic signals from the overall polarization, and discuss in detail the simplifications that arise when the usual assumptions (i.e., weak laser fields, nonoverlapping pulses, slowly varying envelope assumption, and rotating-wave approximation) are invoked. The theoretical considerations are illustrated by nonperturbative calculations of the polarizations and PP signals for a one-dimensional shifted harmonic oscillator.

The capability of the approach is demonstrated by three-dimensional wave-packet calculations for a model system with vibronically coupled PE surfaces, which describes ultrafast nonadiabatic isomerization dynamics triggered by the twisting of a double bond.<sup>21,26</sup> We perform calculations for pulses up to 40 fs duration and obtain for this model frequency-integrated and dispersed PP spectra. We show that these PP signals can be related to field-free molecular observables. In particular, it is demonstrated that the time- and frequency-resolved PP signals reflect in real time the disappearance of the reactants and the delayed appearance of the products. Both populations exhibit oscillations which reflect coherent vibrational motion.

## II. SPECTROSCOPIC SIGNALS

There exists a large variety of spectroscopic techniques that employ ultrashort laser pulses. These methods, which

differ, e.g., in the detection scheme and in the number and properties of laser fields, monitor different aspects of the photodynamics of the molecular system. For example, we may either directly detect the emitted polarization ( $\propto \mathbf{PP}^*$ , so-called homodyne detection), thus measuring the decay of the electronic coherence via the photon-echo effect, or we may employ a heterodyne detection scheme ( $\propto \mathbf{EP}^*$ ), and observe the absorption of the laser field by the sample owing to stimulated emission and resonance Raman processes. Although in principle any of these spectroscopic signals are readily obtained once the electric polarization has been calculated, we will focus in this paper mainly on the discussion of standard PP spectroscopy, i.e., transient transmission (absorption) of a laser pulse in a polarized medium. For an excellent survey of spectroscopic techniques, see a recent article of Mukamel, Fleming and co-workers.<sup>25</sup>

The definition of time- and frequency-resolved PP signals has been discussed recently,<sup>15,16</sup> and is considered here briefly to clarify the approximations involved. We are concerned with the interaction of a molecular system with the electric field  $\mathbf{E}(\mathbf{x}, t)$ , which is considered as an external classical field. Adopting furthermore the electric dipole approximation, the response of the medium is completely described by the electric polarization  $\mathbf{P}(\mathbf{x}, t)$ , which is defined as the expectation value of the electronic dipole moment of the system.<sup>24</sup> To properly describe the propagation of the classical field  $\mathbf{E}(\mathbf{x}, t)$  through the medium characterized by  $\mathbf{P}(\mathbf{x}, t)$ , we have to solve Maxwell's equations for  $\mathbf{E}(\mathbf{x}, t)$  and the Schrödinger equation for  $\mathbf{P}(\mathbf{x}, t)$  in a self-consistent way.<sup>27</sup> In many cases, however, it is justified to circumvent the explicit solution of Maxwell's equations by assuming an optically thin sample, i.e., the incident electric field that induces the polarization passes, by definition, through the medium unchanged. Hence the total electric field at the end of the sample is simply given as a sum of the incident field and the polarization, both propagating in space as plane waves

$$\mathbf{E}_{\text{tot}}(\mathbf{x}, t) = \sum_i \mathbf{E}_i(\mathbf{x}, t) + \sum_N \mathbf{P}^{(N)}(\mathbf{x}, t), \quad (2.1)$$

$$\mathbf{E}_i(\mathbf{x}, t) = E_i(t) \exp(i\mathbf{k}_i \mathbf{x}) + \text{c.c.}, \quad (2.2)$$

$$\mathbf{P}^{(N)}(\mathbf{x}, t) = \sum_{n,m} P_{nm}^{(N)}(t) \exp(i(n\mathbf{k}_1 + m\mathbf{k}_2) \mathbf{x}) + \text{c.c.} \quad (2.3)$$

Here the incident electric field  $\mathbf{E}(\mathbf{x}, t)$  is expressed as sum of several (usually two) laser pulses  $E_i(t) = \boldsymbol{\epsilon}_i E_i(t) e^{-i\omega_i t}$ , each one characterized by its wave vector  $\mathbf{k}_i$ , laser frequency  $\omega_i$ , polarization vector  $\boldsymbol{\epsilon}_i$ , and pulse envelope function  $E_i(t)$ . The individual contributions to the overall polarization  $\mathbf{P}(\mathbf{x}, t)$  characterize the response of the system to  $N$ th order in the incident fields  $\mathbf{E}_i(\mathbf{x}, t)$ , and propagate along the wave vectors  $\mathbf{k}_i$  of these fields as well as linear combinations of them (see Sec. III). To simplify the notation, we henceforth suppress the  $\mathbf{x}$  dependence of  $\mathbf{E}$ ,  $\mathbf{P}$ . Note that the first two approximations employed (classical external field and dipole approximation) are usually well justified in molecular physics, whereas the validity of the assumption of an optically thin sample depends on the specific experiment under consideration.

In a typical PP experiment the pump pulse (field  $\mathbf{E}_1(t)$ ) prepares at  $t=0$  a nonstationary vibrational state on an excited electronic PE surface, which is interrogated after a delay time  $\Delta t$  by the probe pulse (field  $\mathbf{E}_2(t)$ ). The experimental PP signal is usually defined as the difference between the transmittance of the probe pulse with and without the preparation of the sample by the pump pulse. From classical electrodynamics it is well known that the rate of dissipated energy of an electric field  $\mathbf{E}(t)$  in a medium that is characterized by its polarization  $\mathbf{P}(t)$  is given by  $\mathbf{E}(t) \cdot \dot{\mathbf{P}}(t)$ .<sup>24</sup> Assuming a photodetector at the end of the sample that counts all photons being emitted in  $\mathbf{k}_2$  direction, the PP signal is proportional to the total energy dissipated (or gained) by the probe pulse in the medium

$$I = \int_{-\infty}^{\infty} dt \dot{\mathbf{E}}_2(t) \cdot \mathbf{P}(t). \quad (2.4)$$

Here  $\mathbf{P}(t) = \mathbf{P}_{\text{pump on}} - \mathbf{P}_{\text{pump off}}$  denotes the difference of the polarizations radiating along  $\mathbf{k}_2$  with and without the preparation of the sample by the pump pulse, and we have performed a partial integration. The sign convention is such that the signal is negative for absorption (disappearance of photons) and positive for emission (creation of photons). The signal (2.4) depends on the pulse delay time  $\Delta t$  as well as on the properties of the laser pulses (e.g., pulse durations  $\tau_i$  and laser frequencies  $\omega_i$ ), and is often considered as time- and frequency-resolved signal  $I(\omega_2, \Delta t)$  when plotted as a function of  $\Delta t$  and the probe carrier frequency  $\omega_2$ . As Eq. (2.4) is (inherently) integrated over all emission frequencies, it will be referred to as *integral* PP signal.

In order to obtain the spectrum of the emitted field, one has to disperse the probe pulse with a spectrometer after it has passed the sample. Because the PP signal is measured as the time-integrated energy rate (cf. Eq. (2.4)), the corresponding spectrum may be considered as stationary although it inherently depends on the delay time  $\Delta t$ . In this case the effects of the spectrometer need not to be considered in the theoretical description,<sup>28</sup> and we may define the dispersed PP signal as the intensity of the Fourier transform of the total emitted field (2.1), yielding<sup>15,16</sup>

$$I(\omega, \Delta t) = 2\omega \operatorname{Im} \mathbf{E}_2(\omega) \mathbf{P}^*(\omega), \quad (2.5)$$

where

$$\mathbf{E}_2(\omega) = \int_{-\infty}^{\infty} dt e^{i\omega t} \mathbf{E}_2(t), \quad (2.6)$$

$$\mathbf{P}(\omega) = \int_{-\infty}^{\infty} dt e^{i\omega t} \mathbf{P}(t) \quad (2.7)$$

denote the Fourier transform of the incident probe field and the polarization difference  $\mathbf{P}_{\text{pump on}} - \mathbf{P}_{\text{pump off}}$ , respectively. Combining the definitions (2.4)–(2.7), it is easily verified that integration of the dispersed PP signal (2.5) over all emission frequencies  $\omega$  again yields the integral PP signal (2.4). It should be noted that the experimental transmittance spectrum is often defined by normalizing the dispersed PP spectrum (2.5) to the intensity of the incident field,<sup>7,11,16</sup> thus yielding a signal proportional to  $\operatorname{Im} \mathbf{P}(\omega)/\mathbf{E}_2(\omega)$ .

To make contact with other work,<sup>13–16,19</sup> it is instructive to introduce two approximations commonly used in optical spectroscopy. Inserting Eqs. (2.2) and (2.3) into Eq. (2.4), we obtain for the integral PP spectrum

$$I(\omega_2, \Delta t) = 2\omega_2 \operatorname{Im} \int_{-\infty}^{\infty} dt E_2(t) P^*(t), \quad (2.8)$$

where terms with rapidly oscillating ( $\propto 2\omega_2$ ) integrands have been neglected, i.e., we have employed the rotating-wave approximation (RWA).<sup>29</sup> Furthermore, we have adopted the slowly varying envelope approximation, thus neglecting terms depending on the time derivative of the pulse envelope function.<sup>24</sup> As both approximations may approach the limits of their validity in the case of intense femtosecond laser pulses with optical frequencies, all computational results in Sec. IV have been obtained using the complete signal (2.4). It should be noted, however, that in the cases considered the deviations between the complete signal (2.4) and the first term of Eq. (2.8) are minor.

The definitions of the dispersed transmittance spectrum  $I(\omega, \Delta t)$  (Eq. (2.5)) and the integral transmittance spectrum  $I(\omega_2, \Delta t)$  (Eq. (2.4)) connect these experimental signals to the macroscopic polarization difference  $\mathbf{P}(t)$ . By virtue of the assumption of an optically thin sample, both the incident electric fields and the polarization are approximated by plane waves in  $\mathbf{x}$  space, i.e., the macroscopic polarization is simply given by an orientational average over the microscopic polarizations of the individual molecules in a unit volume. Describing the molecular system as an electronic two-state system, the orientational averaging of  $\mathbf{P}(t)$  simply amounts to the multiplication with a constant, i.e., the macroscopic and microscopic polarizations are proportional to each other. Assuming, on the other hand, a model system with several ( $\geq 3$ ) optically bright electronic states, the averaging process depends on the relative orientations of the individual transition dipole moments. In this case it is necessary to perform explicitly the orientational average.<sup>30</sup>

We note in passing that within the assumption of an optically thin sample (and only then) one obtains equivalent expressions for the spectroscopic signals if one starts the derivation from a “system point of view” instead of the “electric field point of view” adopted above. In the former approach, adopted by several workers,<sup>13,14,19,22</sup> one considers the time derivative of the expectation value of the total Hamiltonian  $H(t)$  (consisting of the molecular system  $H_M$  and the field-matter interaction Hamiltonian  $H_{\text{int}}(t)$ , cf. Eq. (3.2)), yielding

$$d/dt \langle H(t) \rangle = -\dot{\mathbf{E}}(t) \cdot \mathbf{P}(t). \quad (2.9)$$

A comparison of Eqs. (2.4) and Eq. (2.9) reassures that the energy loss of the molecular system, given by the time integration over Eq. (2.9), is identical to the energy gain of the electric field (2.4).

Let us finally give an example of a homodyne-detected coherent spectroscopic technique and consider the two-pulse photon-echo signal

$$S(\Delta t) = \int_{-\infty}^{\infty} d\tau |\mathbf{P}_{2\mathbf{k}_2 - \mathbf{k}_1}(\tau, \Delta t)|^2, \quad (2.10)$$

which is given by the time-integrated coherent emission in the background-free direction  $2\mathbf{k}_2 - \mathbf{k}_1$ . Applying fluorescence upconversion techniques with sub-picosecond time resolution, it is possible to monitor in addition to Eq. (2.10) the time evolution of the emission,<sup>31</sup> yielding the two-time photon-echo signal

$$S(\tau, \Delta t) = |\mathbf{P}_{2\mathbf{k}_2 - \mathbf{k}_1}(\tau, \Delta t)|^2. \quad (2.11)$$

### III. EVALUATION OF THE NONLINEAR POLARIZATION

#### A. General aspects

To calculate the electronic polarization, needed for the evaluation of the PP signals defined above, we have to solve the time-dependent Schrödinger equation for the total Hamiltonian  $H(t)$  ( $\hbar = 1$ )

$$i \frac{\partial}{\partial t} |\Psi(t)\rangle = H(t) |\Psi(t)\rangle, \quad (3.1)$$

where  $H(t)$  consists of the molecular Hamiltonian  $H_M$  and the interaction Hamiltonian  $H_{\text{int}}(t)$ . Assuming a coupled two-state model with diabatic<sup>32</sup> electronic states  $|\psi_0\rangle$  and  $|\psi_1\rangle$ , and within the electric dipole approximation, the total Hamiltonian reads

$$H(t) = H_M + H_{\text{int}}(t), \quad (3.2)$$

$$H_M = \sum_{k=0,1} |\psi_k\rangle h_k \langle \psi_k| + \{ |\psi_0\rangle V_{01} \langle \psi_1| + \text{h.c.} \}, \quad (3.3)$$

$$H_{\text{int}}(t) = - |\psi_0\rangle \boldsymbol{\mu}_{01} \cdot \mathbf{E}(t) \langle \psi_1| + \text{h.c.} \quad (3.4)$$

Here  $h_k$  represents the vibrational Hamiltonian of the diabatic electronic basis state  $|\psi_k\rangle$ ,  $V_{01}$  is the diabatic coupling between the electronic states  $|\psi_0\rangle$  and  $|\psi_1\rangle$ , and  $\boldsymbol{\mu}_{01}$  denotes the electronic transition dipole moment. Initially, i.e., before the interaction with the laser field, the molecular system is assumed to be in its electronic and vibrational ground state

$$|\Psi^{(0)}(t)\rangle = e^{-iH_M t} |\Psi_0\rangle, \quad (3.5)$$

where  $|\Psi_0\rangle$  denotes the ground-state wave function of the coupled  $S_0$ - $S_1$  problem.

By solving the Schrödinger equation (3.1) in a nonperturbative manner, we obtain the overall polarization  $\mathbf{P}(t)$  as quantum-mechanical expectation value of the dipole operator

$$\begin{aligned} \mathbf{P}(t) &= \langle \Psi(t) | \boldsymbol{\mu} | \Psi(t) \rangle \\ &= 2 \operatorname{Re} \langle \Psi(t) | \psi_0 \rangle \boldsymbol{\mu}_{01} \langle \psi_1 | \Psi(t) \rangle. \end{aligned} \quad (3.6)$$

As explained above, the overall polarization consists of several contributions

$$\mathbf{P}(t) = 2 \operatorname{Re} \sum_{n,m} P_{n,m}(t) \exp(i(n\mathbf{k}_1 + m\mathbf{k}_2) \cdot \mathbf{x}), \quad (3.7)$$

which can be discriminated experimentally by the direction  $\mathbf{k} = n\mathbf{k}_1 + m\mathbf{k}_2$  in which the emission is observed. To be able to simulate and explain experimental data, we therefore need to (i) specify the individual contributions to the electric po-

larization and the corresponding emission directions (Sec. III B) and (ii) find a method which allows us to extract these contributions from a nonperturbative calculation (Sec. III C).

#### B. Directional dependence of the nonlinear response

The individual contributions to the electric polarization are most naturally obtained in a perturbative treatment of the field-matter interaction. Writing the time-dependent wave function as

$$|\Psi(t)\rangle = \sum_{N=0}^{\infty} |\Psi^{(N)}(t)\rangle, \quad (3.8a)$$

$$|\Psi^{(N)}(t)\rangle = i \int_{-\infty}^t dt' e^{-iH_M(t-t')} \boldsymbol{\mu} \cdot \mathbf{E}(t') |\Psi^{(N-1)}(t')\rangle, \quad (3.8b)$$

we obtain for the polarization

$$\mathbf{P}(t) = \sum_{N=0}^{\infty} \mathbf{P}^{(2N+1)}(t), \quad (3.9a)$$

$$\begin{aligned} \mathbf{P}^{(2N+1)}(t) &= 2 \operatorname{Re} \sum_{i=0}^N \langle \Psi^{2(N-i)}(t) | \psi_0 \rangle \boldsymbol{\mu}_{01} \\ &\quad \times \langle \psi_1 | \Psi^{(2i+1)}(t) \rangle. \end{aligned} \quad (3.9b)$$

Owing to the initial condition (3.5), the linear ( $\mathbf{P}^{(1)}$ ) and third-order ( $\mathbf{P}^{(3)}$ ) polarizations are the first nonvanishing terms of the expansion. The total number of nonzero terms occurring in Eq. (3.9) depends crucially on whether the following conditions are fulfilled:

(i) Rotating-wave approximation: Within the RWA<sup>29</sup> only resonant optical transitions (e.g.,  $\propto e^{i(\omega - h_1)t}$ ) are considered, whereas nonresonant transitions (e.g.,  $\propto e^{i(\omega + h_1)t}$ ) are disregarded. This reduces the number of terms by a factor of 2 in each order of expansion (3.8).

(ii) Nonoverlapping laser pulses: If the laser fields do not overlap in time, we need to consider only one electric field  $\mathbf{E}_i(t)$  in each time integration (3.8b) instead of two. When speaking of nonoverlapping pulses, we will always assume that the pump field  $\mathbf{E}_1$  arrives before the probe field  $\mathbf{E}_2$ .

(iii) Weak-field limit: In the case of small laser intensities it is sufficient to consider the nonlinear response only to lowest (i.e., third) order.

(iv) Phase-averaged detection: If the spectral signals (e.g., Eqs. (2.4) and (2.5)) are averaged over many laser shots (as it is the case in common PP experiments), only signals proportional to  $\mathbf{E}_1^{2n} \mathbf{E}_2^{2m}$  survive the inherent averaging over the individual phases of the fields.<sup>33</sup> Using phase-locked pulses,<sup>25</sup> however, it is also possible to monitor signals proportional to  $\mathbf{E}_1^{2n+1} \mathbf{E}_2^{2m+1}$ . Owing to the definition of the laser fields in Eq. (2.2), the pulses are phase-locked in a numerical simulation of a PP experiment, i.e., phase-sensitive signals in odd order in the electric fields do contribute.

In the most general case (i.e., when none of the assumptions above hold) it is clear that we get an enormous number of contributions and corresponding emission directions  $\mathbf{k}$  in

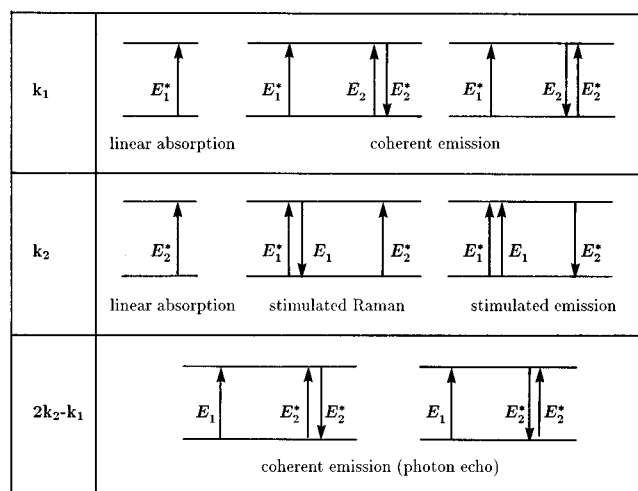


FIG. 1. Diagrammatic representation of various spectroscopic processes that contribute to the electric polarization up to third order. Assuming nonoverlapping pump ( $E_1$ ) and probe ( $E_2$ ) laser fields within the RWA, we obtain, regardless of the laser intensities, only emission into the directions  $\mathbf{k}_1$ ,  $\mathbf{k}_2$ , and  $2\mathbf{k}_2 - \mathbf{k}_1$ .

expansion (3.9). Employing the RWA, however, it is shown in Appendix A that the polarization of  $(2N+1)$ th order only radiates into the directions

$$\mathbf{k} = j(\mathbf{k}_2 - \mathbf{k}_1) + \mathbf{k}_2 \quad (3.10)$$

where  $j$  runs from  $-(N+1)$  to  $N$ . As a direct consequence of Eq. (3.10), we obtain in linear response only emission into  $\mathbf{k}_1$  and  $\mathbf{k}_2$  directions, while the third-order polarizations may radiate along the directions  $\mathbf{k}_1$ ,  $\mathbf{k}_2$ ,  $2\mathbf{k}_2 - \mathbf{k}_1$ , and  $2\mathbf{k}_1 - \mathbf{k}_2$ . Assuming furthermore nonoverlapping pulses, it is easy to show that, even *in arbitrary order of the radiation field*, there is only emission into the directions  $\mathbf{k}_1$ ,  $\mathbf{k}_2$ , and  $2\mathbf{k}_2 - \mathbf{k}_1$  (i.e., regardless of  $N$ ,  $j = -1, 0, 1$ ).

To illustrate these considerations and to elucidate the origin of the individual contributions, Fig. 1 shows a diagrammatic representation of various spectroscopic processes contributing to the electric polarization up to third order.<sup>24,34</sup> In the case of nonoverlapping pulses and within the RWA, the evaluation of Eq. (3.9) yields two terms of the linear polarization propagating in  $\mathbf{k}_1$  and  $\mathbf{k}_2$  directions, and six, eight, and two terms of the third-order polarization propagating in  $\mathbf{k}_1$ ,  $\mathbf{k}_2$ , and  $2\mathbf{k}_2 - \mathbf{k}_1$  direction, respectively. In addition to the diagrams shown in Fig. 1, we moreover get four terms  $\propto E_i^3$  that are independent of  $\Delta t$ , and also two terms in  $\mathbf{k}_2$  which are obtained from the ones shown by simple permutations of the electric fields. The horizontal bars in each diagram represent the ground and excited electronic states of the two-state system (3.3), respectively, and the arrows correspond to electronic transitions due to the electric fields  $E_i$  and their complex conjugates, while the time moves forward from left to right. As discussed in Sec. II, polarizations are experimentally measured by using either a homodyne ( $\propto |P|^2$ ) or a heterodyne ( $\propto P^* E_2$ ) detection scheme, i.e., the (heterodyne) PP signals defined above (Eqs. (2.4) and (2.5)) are obtained by adding an interaction with the probe field  $E_2$  at the right side of each diagram.

Let us first consider the diagrams in  $\mathbf{k}_2$  direction, describing the stimulated Raman and the stimulated emission contribution, respectively. Note that within the delay time  $\Delta t$  (i.e., after the interaction with the pump) the system propagates in either the electronic ground state (Raman case) or in the excited electronic state (stimulated emission case).<sup>24</sup> As a consequence, it is possible to monitor the electronic population dynamics in a PP experiment.<sup>10</sup> Measuring the transient transmittance of the probe pulse as defined above, the heterodyne-detected signal in  $\mathbf{k}_2$  direction is proportional to  $|E_1|^2 |E_2|^2$ , and will thus show up in a PP experiment with phase-averaged detection.

The contributions in  $\mathbf{k}_1$  and  $2\mathbf{k}_2 - \mathbf{k}_1$  directions, on the other hand, describe the time evolution of the system when it is in an electronic coherence. Coherent spectroscopic techniques such as photon-echo measurements usually employ a homodyne detection scheme and monitor the emission in the background-free direction  $2\mathbf{k}_2 - \mathbf{k}_1$ .<sup>24</sup> Being proportional to  $E_1^* |E_2|^2 E_2$  and  $E_1 E_2^* |E_2|^2$ , respectively, the corresponding heterodyne-detected signals are phase-sensitive and therefore only measurable in a PP experiment employing phase-locked laser fields. Moreover, the *linear* polarization in  $\mathbf{k}_1$  leads to a heterodyne signal which is proportional to  $E_1^* E_2$  and thus an explicit function of the pulse delay time  $\Delta t$ .<sup>35</sup> Being a first-order effect, this term is expected to dominate the phase-locked PP signal, but is absent in phase-averaged detection.

As pointed out above, a nonperturbative calculation of the PP signals (2.4) and (2.5) employs phase-locked laser fields. As a consequence the nonperturbative simulation of a PP experiment yields the sum of all contributions discussed above, while a common PP experiment with phase-averaged detection selects only contributions in  $\mathbf{k}_2$  direction.

### C. Nonperturbative evaluation scheme

The basic idea how to determine the directional dependence of the nonlinear polarization in a nonperturbative calculation is rather simple and is most easily demonstrated by an example. Let us again consider nonoverlapping laser fields within the RWA, and let us suppose that we only want to discriminate the (phase-insensitive)  $\mathbf{k}_2$  emission from the (phase-sensitive)  $\mathbf{k}_1$  and  $2\mathbf{k}_2 - \mathbf{k}_1$  contributions. Rewriting the overall polarization as

$$P(\phi) = \sum_n P_n \exp(in\phi), \quad (3.11)$$

where  $n\phi = n\mathbf{k}_1 \mathbf{x}$  denotes the phase the polarization acquires through the interaction with the pump field, it is clear that the terms  $P_{-1}$ ,  $P_0$ , and  $P_1$  represent the polarization in  $2\mathbf{k}_2 - \mathbf{k}_1$ ,  $\mathbf{k}_2$ , and  $\mathbf{k}_1$  directions, respectively. Performing two separate calculations of the overall polarization  $P(\phi)$  employing the phases  $\phi_1 = 0, \phi_2 = \pi$ , it is easy to see that the polarizations in  $\mathbf{k}_2$  and  $\mathbf{k}_1$ ,  $2\mathbf{k}_2 - \mathbf{k}_1$  are given by the linear combinations

$$\mathbf{P}_{\mathbf{k}_2} = \text{Re}\{P(0) + P(\pi)\}, \quad (3.12a)$$

$$\mathbf{P}_{\mathbf{k}_1, 2\mathbf{k}_2 - \mathbf{k}_1} = \text{Re}\{P(0) - P(\pi)\}. \quad (3.12b)$$

As a second example, allow for overlapping laser fields within the RWA and ask for the polarizations up to third

order into all possible directions, i.e., into  $\mathbf{k}_2$ ,  $\mathbf{k}_1$ ,  $2\mathbf{k}_2 - \mathbf{k}_1$ , and  $2\mathbf{k}_1 - \mathbf{k}_2$ . The calculation of the overall polarization  $P(\phi)$  for the phases  $\phi_k = k\pi/2$  ( $k=0,1,2,3$ ) yields a linear system of four equations for the  $P_n$  in Eq. (3.11), the solution of which yields the desired polarizations

$$\mathbf{P}_{\mathbf{k}_2} = \frac{1}{2} \text{Re}\{P(0) + P(\pi/2) + P(\pi) + P(3\pi/2)\}, \quad (3.13a)$$

$$\mathbf{P}_{\mathbf{k}_1} = \frac{1}{2} \text{Re}\{P(0) - P(\pi)\} + \frac{1}{2} \text{Im}\{P(\pi/2) - P(3\pi/2)\}, \quad (3.13b)$$

$$\mathbf{P}_{2\mathbf{k}_2 - \mathbf{k}_1} = \frac{1}{2} \text{Re}\{P(0) - P(\pi)\} + \frac{1}{2} \text{Im}\{P(3\pi/2) - P(\pi/2)\}, \quad (3.13c)$$

$$\mathbf{P}_{2\mathbf{k}_1 - \mathbf{k}_2} = \frac{1}{2} \text{Re}\{P(0) - P(\pi/2) + P(\pi) - P(3\pi/2)\}. \quad (3.13d)$$

From the examples above the generalization of the procedure to cases including arbitrary nonlinear processes of any order is straightforward. To calculate the contributions of the polarization in  $N$  directions, one has to perform  $N$  calculations of the overall polarization  $P(\phi)$  with different phases  $\phi$ , and solve the resulting linear system of equations for the  $P_n$  in (3.11). Beyond the RWA, however, one needs to generalize the ansatz (3.11) and “tag” both the interactions with the pump and the probe fields with phases  $\phi^{(1)} = \mathbf{k}_1 \mathbf{x}$  and  $\phi^{(2)} = \mathbf{k}_2 \mathbf{x}$ , respectively, thus performing a two-dimensional Fourier analysis of the overall polarization.

Analogous to experiment, we thus obtain the nonlinear response of the molecular system resolved in the directions of emission, but summed up over all contributions in each direction. Assuming nonoverlapping laser fields within the RWA, it is possible, moreover, to separate the PP signals arising from the stimulated Raman and the stimulated emission contribution, respectively (see Appendix B). This important feature, which is rather helpful in the interpretation of complex PP spectra (see below), stems from the fact that after the interaction with the pump pulse we may separately consider the electronic ground state component  $\langle \psi_0 | \Psi(t) \rangle$  or excited state component  $\langle \psi_1 | \Psi(t) \rangle$  of the total wave function.<sup>21</sup>

### D. Example: The one-dimensional harmonic oscillator

Before proceeding to a nontrivial application, it is instructive to demonstrate the computational procedure outlined above for the case of a simple and well-understood model problem. Let us consider a one-dimensional harmonic oscillator which is characterized by its vibrational period  $T = 2\pi/\omega = 65$  fs and the dimensionless coordinate shift  $\kappa/\omega = 2$ , describing the displacement of the excited-state geometry with respect to the electronic ground-state geometry. We furthermore assume Gaussian laser pulses of duration  $\tau_1 = \tau_2 = 10$  fs that are resonant with the optical transition (i.e.,  $\omega_1 = \omega_2 = E_1 - E_0 = 3$  eV), and choose the amplitudes of the field-matter interactions as  $|\boldsymbol{\mu} \cdot \mathbf{E}_1| = 0.04$  eV and  $|\boldsymbol{\mu} \cdot \mathbf{E}_2| = 0.01$  eV, respectively. This results in a excited-state population of 7% after the preparation of the system by the pump pulse.

For this model, Fig. 2 shows the modulus of various contributions to the electronic polarization, plotted as a function of the delay time  $\Delta t$  and the emission time after the

probe pulse  $\tau = t - \Delta t$ . The overall polarization shown in Fig. 2(a) is clearly dominated by the linear response of the system. The linear response to the probe field  $\mathbf{E}_2$  manifests itself as wave trains traveling parallel to the  $\Delta t$  axis. The corresponding emission is peaked at times  $\tau = nT = 0, 65, 130$  fs... (clearly seen for  $\Delta t < 0$ , where the  $\mathbf{E}_2$  emission does not yet interfere with the  $\mathbf{E}_1$  emission). Due to the  $\mathbf{P}(\Delta t, t - \Delta t)$  representation chosen, the linear response to the pump field  $\mathbf{E}_1$  results in wave trains traveling diagonally from right to left. In order to distinguish linear and nonlinear response, we calculate the polarizations for the cases that only the pump pulse or the probe pulse interacts with the system, respectively, and subtract these polarizations from the overall polarization. This yields the total nonlinear polarization  $\mathbf{P}_{\text{NL}} = \mathbf{P}_{\text{tot}} - \mathbf{P}_{\text{pump only}} - \mathbf{P}_{\text{probe only}}$  as shown in Fig. 2(b). The total nonlinear polarization  $\mathbf{P}_{\text{NL}}$  is about a factor of 20 weaker than the overall polarization  $\mathbf{P}_{\text{tot}}$  shown in Fig. 2(a), where it is only noticeable as little humps on top of the wave trains. The emission is mainly peaked at delay times and emission times  $\Delta t, \tau = nT$ , but also exhibits complex additional structures, arising from the superposition of the individual contributions to the polarization  $\mathbf{P}_{\text{NL}}$ .

Employing the computational procedure defined by Eq. (3.13), we finally obtain the direction-resolved polarizations, radiating in directions  $\mathbf{k}_1$ ,  $\mathbf{k}_2$ ,  $2\mathbf{k}_2 - \mathbf{k}_1$ , and  $2\mathbf{k}_1 - \mathbf{k}_2$  [Figs. 2(c)–2(f)], respectively. It should be emphasized that for the field intensities considered here, the RWA as well as the assumption of only 4 directions of the emission (cf. Eq. (3.10)) represent excellent approximations. As the probe field is taken to be a factor of four weaker than the pump field, the contributions proportional to  $\mathbf{E}_1 \mathbf{E}_2^2$  (i.e.,  $\mathbf{P}_{\mathbf{k}_1}, \mathbf{P}_{2\mathbf{k}_2 - \mathbf{k}_1}$ ) are consequently also roughly by a factor 4 smaller than the contributions proportional to  $\mathbf{E}_2 \mathbf{E}_1^2$  (i.e.,  $\mathbf{P}_{\mathbf{k}_2}, \mathbf{P}_{2\mathbf{k}_1 - \mathbf{k}_2}$ ). Note, furthermore, that the first peaks (i.e., for  $\tau \approx 0$ ) are somewhat smaller than the following ones (for  $\tau \approx nT$ ), owing to the fact that the polarization still needs to be built up during the interaction with the probe field.

The polarizations  $\mathbf{P}_{2\mathbf{k}_2 - \mathbf{k}_1}$  and  $\mathbf{P}_{2\mathbf{k}_1 - \mathbf{k}_2}$  represent the well-known two-pulse photon-echo emission, emerging for  $\Delta t \geq 0$  in direction  $2\mathbf{k}_2 - \mathbf{k}_1$  and for  $\Delta t \leq 0$  in direction  $2\mathbf{k}_1 - \mathbf{k}_2$ .<sup>13,25</sup> The name photon echo refers to the recurrences (echos) exhibited at times  $\tau = \Delta t = nT$ , reflecting the coherent rephasing of the emission. In the case of an undamped harmonic oscillator (i.e., in the absence of any dephasing processes), the system dynamics is harmonic, and one therefore obtains rephasings whenever  $\tau$  or  $\Delta t$  equals multiples of the vibrational period  $T$ . The polarizations radiating in  $\mathbf{k}_1$  and  $\mathbf{k}_2$  are seen to exhibit more complicated structures, which arise from the fact that several spectroscopic processes contribute in these directions. Recalling the discussion of Fig. 1, we obtain coherent emission in  $\mathbf{k}_1$  direction, while the (phase-insensitive) emission in  $\mathbf{k}_2$  direction consists of the stimulated Raman and stimulated emission contributions. The complex structures arising when the probe pulse is co-incident with or ahead of the pump pulse correspond to the

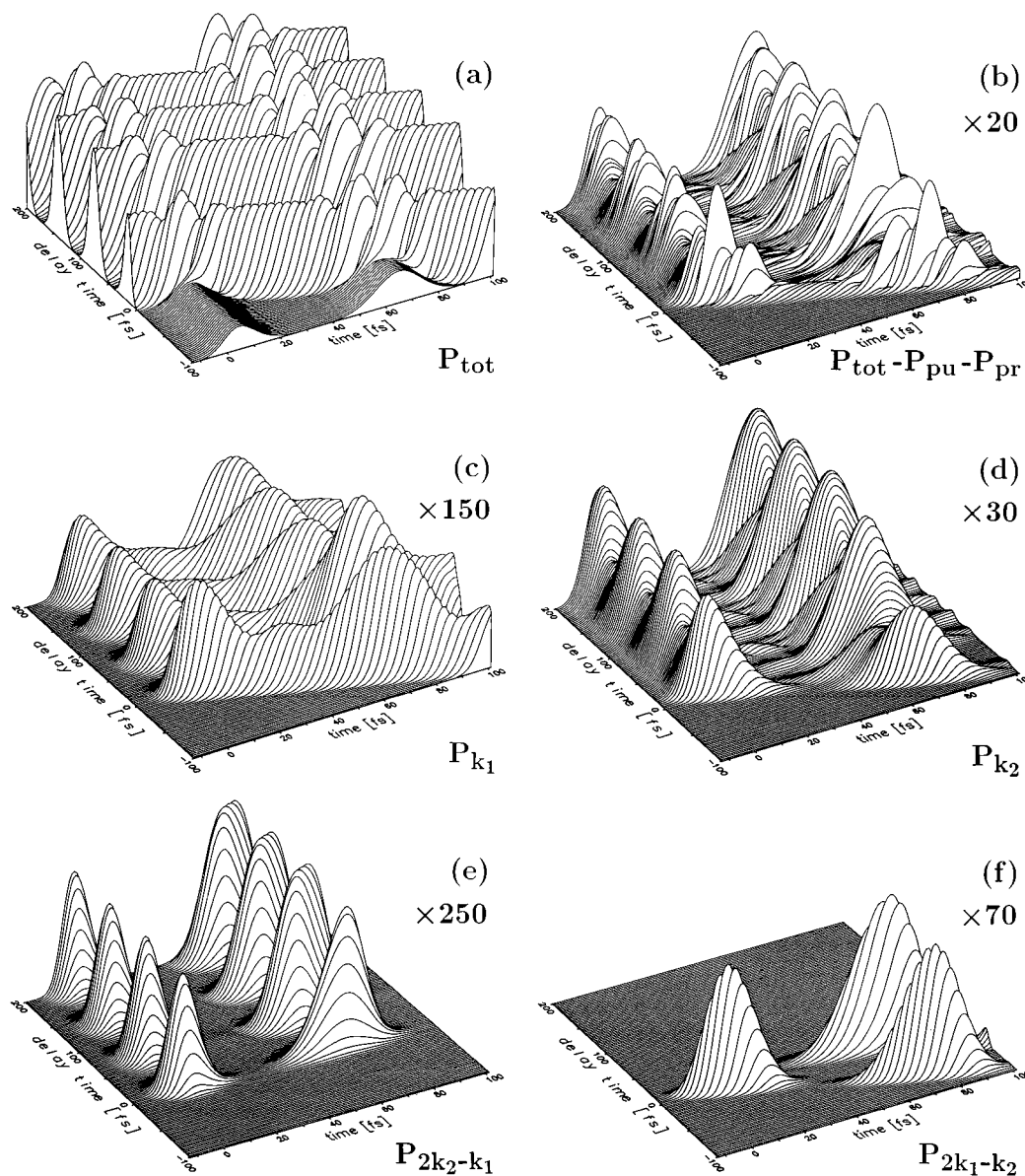


FIG. 2. Modulus of various contributions to the electronic polarization for a one-dimensional shifted harmonic oscillator, plotted as a function of the delay time  $\Delta t$  and the emission time  $\tau = t - \Delta t$ . Panel (a) shows the *overall* polarization  $\mathbf{P}_{\text{tot}}$  as obtained in a nonperturbative calculation, while panel (b) shows the *total nonlinear* polarization which is defined as  $\mathbf{P}_{\text{NL}} = \mathbf{P}_{\text{tot}} - \mathbf{P}_{\text{pump only}} - \mathbf{P}_{\text{probe only}}$ . Assuming weak laser fields within the RWA, the polarization  $\mathbf{P}_{\text{NL}}$  radiates exclusively in four directions. Panels (c) - (f) show the corresponding direction-resolved polarizations radiating in directions  $\mathbf{k}_1$  (c),  $\mathbf{k}_2$  (d),  $2\mathbf{k}_2 - \mathbf{k}_1$  (e), and  $2\mathbf{k}_1 - \mathbf{k}_2$  (f).

so-called coherent artifact, which has been discussed by several authors.<sup>13,16,36</sup>

As pointed out above, the  $\mathbf{k}_2$  emission represents the only contribution to the overall polarization that is measured in a typical PP experiment with phase-averaged detection. To give an example of the connection between polarization and measured PP signal, Fig. 3(a) shows the integral PP spectrum  $I(\omega_2, \Delta t)$  obtained by nonperturbative evaluation of  $\mathbf{P}_{\mathbf{k}_2}$  (for many probe carrier frequencies  $\omega_2$ ) and subsequent time integration over the probe field  $\mathbf{E}_2$  (cf. Eq. (2.4)). As has been discussed by several authors,<sup>10-16</sup> the transient transmittance spectrum monitors the time evolution of the nonstationary wave function prepared by the pump pulse, which manifests

itself through nuclear wave-packet motion in the electronic ground state (Raman contribution) and in the excited electronic state (stimulated emission contribution). As noted above, in the case of nonoverlapping laser fields it is possible to distinguish between these two contributions, thus yielding separately the Raman signal [shown in Fig. 3(b)] and the stimulated emission signal [shown in Fig. 3(c)]. It is seen that the wave-packet motion in the excited electronic state is considerably more pronounced than the wave-packet motion in the ground state. This is due to the fact that the maximal displacement of the ground-state wave-packet is determined by the interaction time with the pump pulse (i.e., for an ideally short pump pulse the Raman contribution becomes



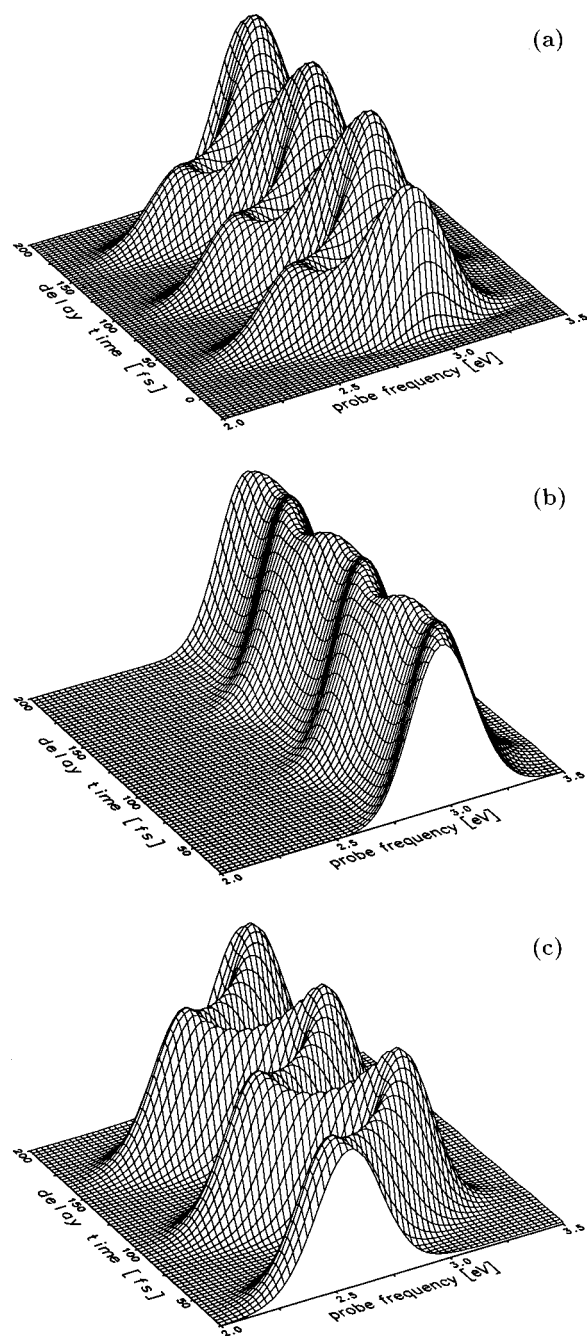


FIG. 3. Integral time- and frequency-resolved PP signals for a one-dimensional shifted harmonic oscillator, obtained for Gaussian laser pulses of 10 fs duration. The total signal (a) consist of the stimulated Raman contribution (b) and the stimulated emission contribution (c).

stationary), while the displacement of the excited-state wave-packet is mainly determined by the coordinate shift of the excited-state geometry, resulting in a maximal redshift of the emission at the classical turning points  $\Delta t = (n + \frac{1}{2})T$ .

Figures 2 and 3 illustrate the nonperturbative approach to calculate PP signals that are simultaneously resolved in frequency, time, and direction of emission. The procedure is straightforward and in clear analogy to experiment, but involves several steps. If one is interested in the spectroscopic response of a harmonic oscillator, one would certainly prefer

the standard perturbative approach, because the corresponding nonlinear response functions can be evaluated analytically.<sup>10,13,16</sup> Considering cases where the description of the molecular system requires a numerical wave-packet propagation, on the other hand, the exact treatment of the field-matter interaction is often more straightforward than the cumbersome numerical evaluation of multi-time system response functions and allows, furthermore, the treatment of strong-field effects.

#### IV. FEMTOSECOND SPECTROSCOPY OF MULTIDIMENSIONAL NONADIABATIC PHOTOISOMERIZATION DYNAMICS

##### A. Model system and computational methods

The photoinduced *cis-trans* isomerization of polyenes and related organic molecules represents a fundamental type of photoreaction.<sup>37</sup> It is generally believed that the twisting about a carbon-carbon double bond leads to a degeneracy or near-degeneracy of the excited electronic state with the ground state. This so-called photochemical funnel is thought to be responsible for an ultrafast internal-conversion (IC) process from the photoexcited state back to the ground state.<sup>37</sup> Although a fairly comprehensive intuitive picture of the photoisomerization dynamics of double bonds has been developed, the theoretical description of these processes has been restricted to simple phenomenological models<sup>38–40</sup> or to one-dimensional (torsional mode only) quantum-mechanical calculations.<sup>41–43</sup>

In a first attempt to account for the multidimensional nature of the dynamics in a truly microscopic manner, Seidner and Domcke have recently proposed a computational treatment of the time-dependent non-Born-Oppenheimer wave-packet dynamics for models which include vibronic coupling of the lowest singlet states ( $S_0, S_1$ ), a large-amplitude torsional mode, as well as one or two accepting modes for the radiationless transition.<sup>26</sup> It has been shown that these models are suitable to reveal basic features of the nonadiabatic photoisomerization process, including the irreversible decay of the electronic population of the initially excited electronic state. Furthermore first simulations of femtosecond PP experiments for such models have been reported.<sup>21,44</sup>

In the present work we consider a three-dimensional model of a photoisomerization process to demonstrate the capability of the nonperturbative approach developed above. The three nuclear degrees of freedom consist of a large-amplitude torsional motion, a vibrational mode of appropriate symmetry which couples the electronic ground state and the excited state (the “coupling mode”), and a totally symmetric mode which modulates the energy gap of the interacting states (the “tuning mode”). Let  $\varphi$  denote the torsional angle, and  $Q_c$  and  $Q_t$  the (dimensionless) normal coordinate of the coupling and the tuning mode, respectively. The diabatic matrix elements of the molecular Hamiltonian (3.3) can then be written as<sup>21</sup>

$$h_k = h + V^{(k)}(\varphi) + \kappa^{(k)} Q_t, \quad (4.1a)$$

TABLE I. Reciprocal moment of inertia  $I^{-1}$  and parameters  $E_k, V_k$  for the torsional potentials, as well as vibrational frequencies  $\omega$  and vibronic coupling constants  $\kappa^{(k)}$  and  $\lambda$  for the harmonic degrees of freedom. All quantities are given in eV.

		$S_0$	$S_1$
Torsional mode $\varphi$	$I^{-1}$	$5 \times 10^{-4}$	$5 \times 10^{-4}$
	$E_k$	0.0	2.75
	$V_k$	5.0	2.5
Tuning mode $Q_t$	$\omega_t$	0.1	0.1
	$\kappa^{(k)}$	0.0	0.1
Coupling mode $Q_c$	$\omega_c$	0.17	0.17
	$\lambda$	0.34	

$$h = -\frac{1}{2I} \frac{\partial^2}{\partial \varphi^2} + \frac{1}{2} \sum_{j=c,t} \omega_j \left\{ Q_j^2 - \frac{\partial^2}{\partial Q_j^2} \right\}, \quad (4.1b)$$

$$V_{01} = \lambda Q_c. \quad (4.1c)$$

Here  $I$  denotes the moment of inertia for the torsional motion,  $\omega_c$  and  $\omega_t$  are the vibrational frequencies of the coupling and tuning mode, respectively,  $\kappa^{(k)}$  represents the gradient of the excited-state PE surface at the ground-state equilibrium geometry, and  $\lambda$  is the vibronic coupling constant. The torsional potentials  $V^{(k)}(\varphi)$  are represented by a Fourier series. Choosing

$$V^{(0)}(\varphi) = E_0 + \frac{1}{2} V_0 (1 - \cos \varphi), \quad (4.2a)$$

$$V^{(1)}(\varphi) = E_1 - \frac{1}{2} V_1 (1 - \cos \varphi), \quad (4.2b)$$

the excited-state potential  $V^{(1)}(\varphi)$  is inverted, i.e., it exhibits a maximum at the ground-state equilibrium geometries ( $\varphi = 0, 2\pi$ ) and a minimum at  $\varphi = \pm\pi$ . The parameters of the model are collected in Table I. For a more detailed discussion of this type of model and the associated multi-dimensional non-Born-Oppenheimer dynamics, we refer to Ref. 26.

As the torsional degree of freedom can be considered to represent the “reaction coordinate” of the system, thus reflecting the chemical aspects of the model, it is instructive to take a look at the torsional potentials shown in Fig. 4. It is

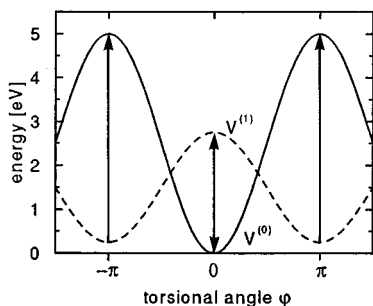


FIG. 4. Diatomic potential energies  $V^{(0)}, V^{(1)}$  as a function of the torsional angle  $\varphi$ , which represents the “reaction coordinate” of the three-dimensional model of photoinduced *cis-trans* isomerization. It is seen that electronic transitions occurring at  $\varphi \approx 0$  (the absorption/emission of the reactants) are resonant to a laser frequencies of  $\approx 2.75$  eV, while electronic transitions occurring at  $\varphi \approx \pm\pi$  (the absorption of the products) are expected for laser frequencies of  $\approx 4.75$  eV.

seen that the two diabatic states interchange upon torsion, i.e., the upper electronic state for  $\varphi = 0$  becomes the lower electronic state for  $\varphi = \pm\pi$ . Contrary to earlier studies,<sup>26</sup> the parameters of the model are chosen such that the vertical electronic energy gap at  $\varphi = 0$  ( $V^{(1)} - V^{(0)} = 2.75$  eV) is smaller than the energy gap at  $\varphi = \pm\pi$  ( $V^{(1)} - V^{(0)} = 4.75$  eV). It is thus clear from Fig. 4 that electronic transitions occurring at  $\varphi \approx 0$  (the absorption of the reactants) should be resonant to a laser frequency of  $\approx 2.75$  eV, while electronic transitions occurring at  $\varphi \approx \pm\pi$  (the absorption of the products) would be expected for laser frequencies of  $\approx 4.75$  eV.

The computational methods have been described in detail elsewhere (see Refs. 26, 45, and 46), and are only sketched here briefly for the sake of completeness. In short, the time-dependent Schrödinger equation (3.1) is converted into a numerically tractable problem by expanding the state vector  $|\Psi(t)\rangle$  in a direct-product basis constructed from diabatic electronic states, free-rotor states for the torsional degree of freedom and harmonic-oscillator states for the remaining vibrational degrees of freedom. Converged results are obtained by truncating the expansion at the maximum quantum numbers  $N_\varphi = 110$ ,  $N_c = 20$ , and  $N_t = 16$ , respectively. This results in a system of 70.400 coupled first-order differential equations

$$i\dot{\mathbf{C}}(t) = \mathbf{H}(t)\mathbf{C}(t), \quad (4.3)$$

where  $\mathbf{H}(t)$  denotes the representation of the total Hamiltonian in the direct-product basis and  $\mathbf{C}(t)$  is the vector of expansion coefficients. The initial-value problem (4.3) has been solved using a Runge-Kutta-Merson scheme with adaptive step size. It is interesting to note that the numerical solution of Eq. (4.3) is, at least in the limit of weak external fields, not more demanding than the solution of the field-free problem (i.e., for  $H_{\text{int}}(t) = 0$ ). This is a consequence of the strong vibronic coupling implying that fast oscillations with a period corresponding to the  $S_0$ - $S_1$  energy gap are already present in the field-free problem. To give an indication of the computer resources required, we note that the calculation of a single point of the integral stimulated spectrum (i.e., for a single delay time  $\Delta t$  and probe frequency  $\omega_2$  and only one propagation performed) takes in the case of 6 fs pulses about 20 s CPU-time on a single processor of the CRAY Y-MP. Considering pulses of 40 fs duration, the corresponding calculation requires 135 CPU s, i.e., the computational time scales almost linearly with the pulse duration.

## B. Time- and frequency-resolved spectroscopy

Employing the three-dimensional model for photoisomerization introduced above, we have performed a series of nonperturbative calculations, considering various wavelength and pulse durations of the laser fields and studying integral and dispersed PP spectra as well as coherent photon-echo signals. In all calculations, it has been assumed that the molecular system undergoes resonant excitation by the pump pulse, i.e.,  $\omega_1 = E_1 - E_0$ . It has been found that the photo-

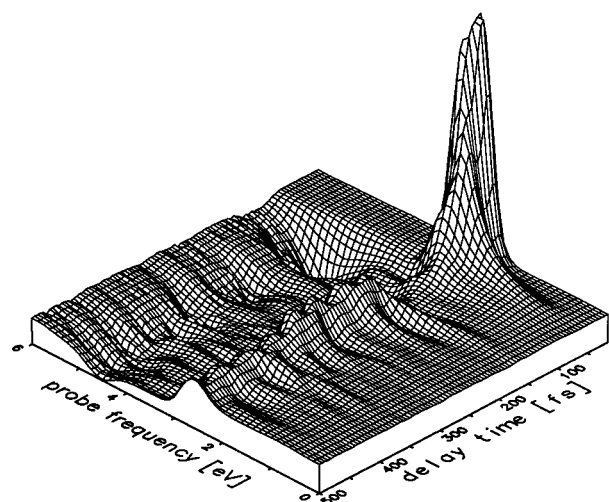


FIG. 5. Integral stimulated-emission PP spectrum for the three-dimensional model of *cis-trans* isomerization, obtained for Gaussian laser pulses of 6 fs duration.

physics exhibited by the model is observed most clearly in the integral stimulated-emission signal for relatively short pulses.

To give a first impression of the photophysics of the system, Fig. 5 shows the time- and frequency-resolved integral PP signal obtained with Gaussian laser pulses of 6 fs duration. As the Raman contribution mainly results in a structureless background emission around  $\omega_2 \approx E_1$  [cf. Fig. 6(a)], it has been subtracted in Fig. 5. For zero delay time  $\Delta t \approx 0$  the PP spectrum resembles the stationary absorption spectrum of the  $S_1$  state. Beginning at  $\Delta t \gtrsim 100$  fs, the PP signal is seen to split up into two components centered at  $\omega_2 \approx 2.5$  eV and  $\omega_2 \approx 4.5$  eV, respectively. As has been anticipated in the discussion of Fig. 4, the first component describes the stimulated emission ( $S_1 \rightarrow S_0$ ) and absorption ( $S_0 \rightarrow S_1$ ) of the reactants, while the latter component describes the absorption ( $S_0 \rightarrow S_1$ ) of the products. Recall that by definition (see Eq. (2.4)) the signal is positive for emission processes and negative for absorption processes. In the following we will refer to the two emission/absorption bands as “reactant channel” and “product channel,” respectively. Note that both channels exhibit quasiperiodic recurrences, reflecting coherent wave-packet motion in the ground and excited electronic states.

To investigate the nonadiabatic photoisomerization dynamics exhibited by the overview spectrum in Fig. 5 in some more detail, let us consider the dispersed PP spectra employing probe frequencies that are resonant to the vertical electronic transition energy of the reactant and product channel, respectively. As it is interesting to study the system response for longer laser pulses, we choose pulses of 40 fs duration in this example. To facilitate convergence, we have employed a Gaussian cut-off function  $\exp(-t^2/\tau^2)$  with  $\tau = 50$  fs when evaluating the Fourier transform of the polarization (2.7). As result, Fig. 6 shows the first picosecond of the time evolution of the corresponding dispersed transmittance spectra, obtained for  $\omega_2 = 2.75$  eV (a) and  $\omega_2 = 4.75$  eV (b), respectively.

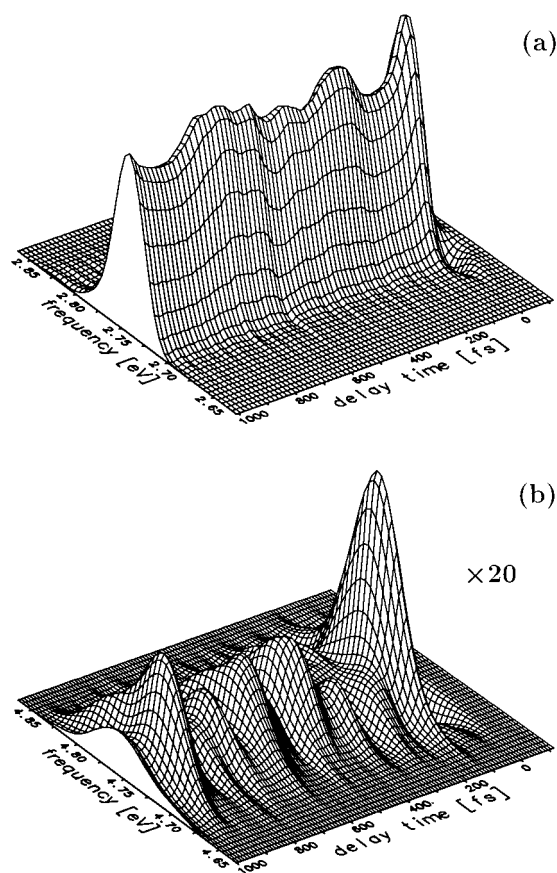


FIG. 6. Dispersed PP spectra for the three-dimensional model of *cis-trans* isomerization, assuming Gaussian pulses of 40 fs duration. In (a) the probe pulse is resonant to the electronic gap at the torsional angle  $\varphi = 0$  ( $\omega_2 = V^{(1)}(0) - V^{(0)}(0) = 2.75$  eV), thus detecting the dynamics of the reactant channel. In (b) the carrier frequency of the probe pulse is  $\omega_2 = V^{(1)} \times (\pi) - V^{(0)}(\pi) = 4.75$  eV, thus detecting the dynamics of the product channel.

The reactant channel (a) is seen to be dominated by the Raman contribution, which manifests itself as broad background emission. The slow beatings in the signal results from the superposition of the Raman and stimulated emission contributions. To better see the coherent response of the product channel, the spectrum in Fig. 6(b) has been inverted and enlarged by a factor of 20. After a somewhat delayed onset, the product channel is seen to exhibit complex structures in time and frequency, reflecting coherent wave-packet motion in the ground state of the product conformation.

It is interesting to study to what extent the nonadiabatic isomerization dynamics, clearly exhibited in the PP signal, is monitored by standard coherent techniques. As an example for the coherent response of the model system, Fig. 7 shows the two-time photon-echo signal (2.11) for 6 fs pulses with frequencies  $\omega_1 = \omega_2 = E_1 - E_0$ . The photon-echo signal exhibits oscillations with the period of the tuning mode ( $T \approx 41$  fs), which are damped on a time scale corresponding to a total electronic dephasing time of  $T_2 \approx 100$  fs. It is interesting to note that Fig. 7 resembles the photon-echo signal for a simple one-dimensional harmonic oscillator that is

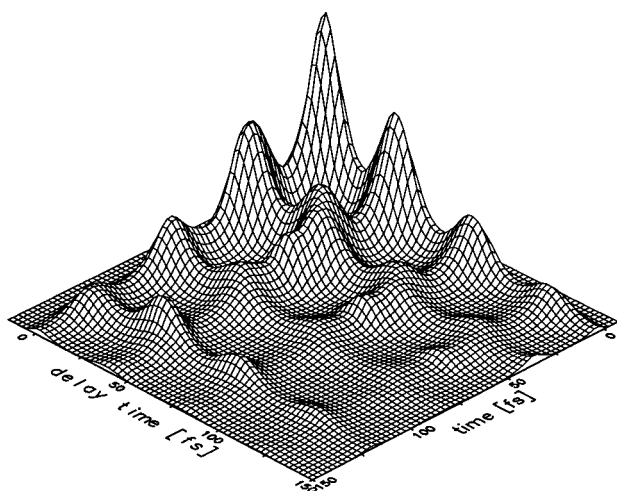


FIG. 7. Two-pulse photon-echo signal for the three-dimensional model of *cis-trans* isomerization, plotted as a function of the delay time  $\Delta t$  and the emission time  $\tau = t - \Delta t$ . We have assumed resonant ( $\omega_1 = \omega_2 = 2.75$  eV) laser pulses of 6 fs duration.

homogeneously broadened,<sup>13,47</sup> i.e., the nonadiabatic isomerization is solely reflected in a generic homogeneous electronic dephasing process.

### C. Interpretation of the PP signals in terms of time-dependent intramolecular observables

Although the overall features of the PP spectra in Figs. 4 and 5 can qualitatively be rationalized in terms of the PE functions shown in Fig. 4, the investigation of the origin of specific features in these spectra requires comprehensive studies of the wave-packet dynamics occurring on coupled PE surfaces. As a simple aid for the interpretation of PP signals of nonadiabatically coupled systems, it has been proven useful to consider time-dependent intramolecular observables, characterizing the electronic and vibrational dynamics of the field-free system.<sup>15,45</sup> As an example, consider

$$P_k^{\text{di}}(t) = \langle \Psi(t) | \hat{P}_k^{\text{di}} | \Psi(t) \rangle, \quad (4.4)$$

$$\hat{P}_k^{\text{di}} = |\psi_k\rangle \langle \psi_k|$$

representing the time-dependent electronic population probability of the *diabatic* state  $|\psi_k\rangle$ . Introducing *adiabatic* electronic basis states  $|\psi_k^{\text{ad}}\rangle$ , we may also evaluate the corresponding *adiabatic* population probability by calculating the expectation value of the projector  $\hat{P}_k^{\text{ad}} = |\psi_k^{\text{ad}}\rangle \langle \psi_k^{\text{ad}}|$ . The diabatic and adiabatic electronic population probabilities describe the decay of the excited electronic state into the electronic ground state and are therefore central quantities in the discussion of vibronic coupling and radiationless relaxation (see Refs. 46, 48–50 for a further discussion).

In the same way, we define the time-dependent probability of finding the system in either the *cis* or the *trans* conformation as the expectation value of the projector<sup>26</sup>

$$\hat{P}_{\text{trans}} = \Theta(|\varphi| - \pi/2), \quad (4.5)$$

$$\hat{P}_{\text{cis}} = \mathbf{1} - \hat{P}_{\text{trans}},$$

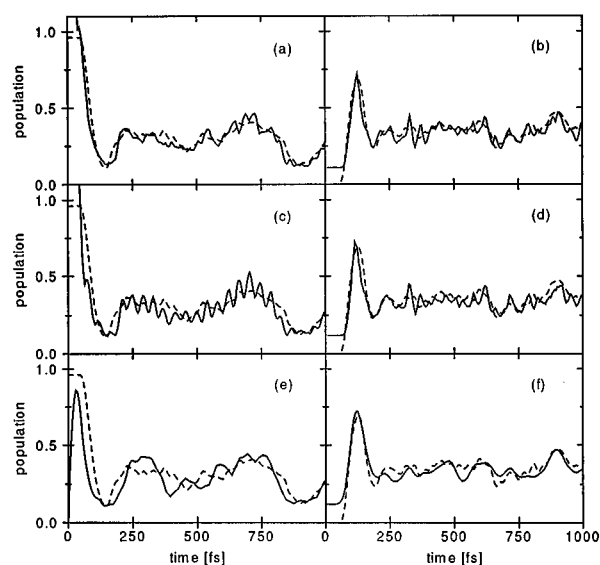


FIG. 8. Comparison of the integral PP signal (solid lines) with the adiabatic population probabilities  $P_{1\text{cis}}^{\text{ad}}(t)$  and  $P_{0\text{trans}}^{\text{ad}}(t)$  (dashed lines). The PP signals on the left side are obtained for probe frequencies resonant to the reactant channel [ $\omega_2 = 2.5$  eV (a), 2.75 eV (a),(e)] and are in good agreement to  $P_{1\text{cis}}^{\text{ad}}(t)$ . The PP signals on the right side are obtained for probe frequencies resonant to the product channel [ $\omega_2 = 4.5$  eV (b), 4.75 eV (d),(f)] and match nicely the population probability  $P_{0\text{trans}}^{\text{ad}}(t)$ . We have assumed Gaussian laser pulses of 6 fs (a),(b) and 40 fs (c)–(f) duration.

where  $\Theta$  denotes the Heaviside step function and  $\varphi$  is restricted to  $-\pi \leq \varphi \leq \pi$ . We may also consider joint population probabilities, e.g., the observables

$$P_{1\text{cis}}^{\text{ad}}(t) = \langle \Psi(t) | \hat{P}_{\text{cis}} \hat{P}_1^{\text{ad}} | \Psi(t) \rangle, \quad (4.6)$$

$$P_{0\text{trans}}^{\text{ad}}(t) = \langle \Psi(t) | \hat{P}_{\text{trans}} \hat{P}_0^{\text{ad}} | \Psi(t) \rangle, \quad (4.7)$$

representing the probability that the system is in the *cis* conformation of the adiabatic excited electronic state (Eq.(4.6)) and in the *trans* conformation of the adiabatic electronic ground state (Eq.(4.7)).

Recall that in the discussion of Figs. 4, 5, and 6 we have attributed the reactant channel (i.e., the emission band at  $\omega_2 \approx 2.5$  eV) to  $S_1 \rightarrow S_0$  stimulated emission close to the equilibrium geometry of the  $S_0$  state (i.e., for  $\varphi = 0$ ). From the definition of the population probability (4.6), it is then intuitively clear that  $P_{1\text{cis}}^{\text{ad}}(t)$  should resemble the stimulated emission of the reactant channel. In the same way it may be expected that the  $S_0 \rightarrow S_1$  absorption of the product channel monitors the population probability  $P_{0\text{trans}}^{\text{ad}}(t)$ .

Figure 8 confirms these conjectures by showing cuts of constant probe frequency of the integral PP spectrum  $I(\omega_2, \Delta t)$  assuming pulses of 6 fs (panels (a)–(d)) and 40 fs duration (panels (e),(f)), respectively. The absolute scale of the PP signals (full curves) is arbitrary; it has been adjusted to match the population probabilities (dashed lines). The PP signals in Figs. 8(a) and 8(b) show cuts that have been obtained at the center of the reactant emission spectrum ( $\omega_2 = 2.5$  eV) and the product absorption spectrum in Fig. 5 ( $\omega_2 = 4.5$  eV), respectively. It is seen that the integral PP signals with 6 fs pulses nicely monitor most of the features of the field-free intramolecular observables  $P_{1\text{cis}}^{\text{ad}}(t)$  and

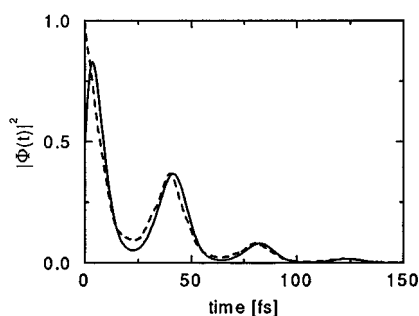


FIG. 9. Time-integrated photon-echo signal (solid line) obtained for resonant 6 fs pulses compared to the squared modulus of the autocorrelation function (dashed line).

$P_{0trans}^{ad}(t)$ . Tuning the probe laser frequency in resonance with the electronic transition energy of the two channels (i.e.,  $\omega_2 = 2.75$  eV (c),  $\omega_2 = 4.75$  eV (d)), the agreement between the PP signals and the population probabilities becomes somewhat worse. In particular, the signal pertaining to the reactant channel exhibits a coherent beating with the frequency of the tuning mode, which is not observed in  $P_{1cis}^{ad}(t)$ . Finally, the comparison of PP signals and population probabilities shown in Figs. 8(e) and 8(f) demonstrates that the qualitative features of  $P_{1cis}^{ad}(t)$  and  $P_{0trans}^{ad}(t)$  are still observable with pulses of 40 fs duration. Owing to the dominant Raman contribution to the reactant signal in the case of longer pulse durations, however, the comparison is worse for  $P_{1cis}^{ad}(t)$ .

Note that all the examples given so far describe different aspects of the electronic *population* dynamics. The time evolution of the electronic *coherence* (i.e., the off-diagonal elements of the electronic density matrix) can be described by the electronic autocorrelation function

$$\Phi(t) = \langle \Psi(t) | \Psi(0) \rangle, \quad (4.8)$$

which is the Fourier transform of the stationary absorption spectrum. Figure 9 compares the squared modulus of the autocorrelation function (dashed line) with the time-integrated photon-echo signal (2.10) (full line) for resonant pulses of 6 fs duration. To facilitate the comparison, we have averaged over the rapid oscillations of  $\Phi(t)$  which correspond to the electronic gap  $E_1 - E_0$ . The time evolution of the autocorrelation function qualitatively matches the decay of the photon echo, confirming that the electronic transition is essentially homogeneously broadened.

## V. CONCLUDING REMARKS

We have proposed a general approach to calculate nonlinear polarizations and the corresponding PP spectra in a nonperturbative manner. We have outlined a practical method to extract the individual contributions to the polarization and the corresponding spectroscopic signals from the overall polarization, and have discussed in detail the simplifications that arise when the usual assumptions (i.e., weak laser fields, nonoverlapping pulses, RWA and slowly varying envelope assumption) are invoked. The resulting computational procedure has been illustrated by nonperturbative cal-

culations of the polarizations and PP signals for a one-dimensional shifted harmonic oscillator. It is noteworthy that in direct analogy to experiment, the nonperturbative approach evaluates time- and frequency-resolved PP spectra point by point. The method is straightforward, easy to implement, and ideally suited for parallel processing.

The capability of the approach has been demonstrated by evaluating the nonlinear polarization for a three-dimensional model system with vibronically coupled PE surfaces, describing ultrafast nonadiabatic isomerization dynamics triggered by the twisting of a double bond. We have considered various wavelength and pulse durations of the laser fields and study integral and dispersed PP spectra as well as coherent photon-echo signals. It has been shown that the approach enables one to simulate realistic PP experiments (i.e., without assuming ideally short, nonoverlapping, and weak laser pulses) for nontrivial molecular model systems (involving multidimensional nuclear dynamics on coupled PE surfaces).

It is tempting to compare the PP simulations for our three-dimensional isomerization model (3.3) to existing experimental investigations on ultrafast *cis-trans* isomerization processes. Using resonant pump pulses of 35 fs duration and probe pulses of variable wavelength and 10 fs duration, Shank and co-workers have obtained time- and frequency-resolved transmittance spectra of the retinal chromophore in rhodopsin.<sup>51</sup> In striking analogy to our Fig. 5, the transient transmittance spectrum of rhodopsin exhibits two separated absorption/emission bands, which were interpreted as the bleaching of the ground-state reactant and the transient absorption of the photoproducts, which are formed within 200 fs.<sup>51</sup> Furthermore Shank and collaborators found that both the reactant channel and the product channel exhibit coherent oscillations of the PP signals, indicating that the photoisomerization of rhodopsin is a vibrationally coherent photochemical reaction.

It is remarkable that many of the overall features of the transient transmittance spectrum of rhodopsin are qualitatively reproduced by the present three-dimensional model. This suggests the interesting possibility that the subpicosecond time evolution of even complex molecular systems may be mainly determined by only a few strongly coupled intramolecular nuclear degrees of freedom rather than by a “bath” of many very weakly coupled vibrational modes. Further progress in the theoretical description of femtosecond spectroscopy of nonadiabatic multimode dynamics (employing, e.g., a semiclassical approach<sup>44,52</sup>) as well as the experimental investigation of smaller molecules should provide new insights into these challenging and fundamental issues of photoinduced relaxation processes.

## ACKNOWLEDGMENTS

This work has been supported by the Deutsche Forschungsgemeinschaft and the Fonds der Chemischen Industrie. Part of the calculations has been performed on a CRAY Y-MP8 at the Leibniz Rechenzentrum der Bayerischen Akademie der Wissenschaften.

## APPENDIX A

The purpose of this Appendix is to derive the number of directions the polarization is emitted in the case of (i) no further approximations, (ii) within the RWA, and (iii) within the RWA and nonoverlapping pulse approximation.

(i) When the nonlinear polarization  $\mathbf{P}^{(2N+1)}(t)$  is evaluated for the most general case, each of the  $2N+1$  interactions with the electric field introduces one of the four phase factors  $e^{\pm i\mathbf{k}_1\mathbf{x}}$ ,  $e^{\pm i\mathbf{k}_2\mathbf{x}}$ , resulting in  $4 \times (2N+1)$  new terms of the polarization (besides the polarizations already obtained in lower orders of the expansion), with wave vectors

$$\mathbf{k} = n\mathbf{k}_1 + m\mathbf{k}_2, \quad |n| + |m| = 2N+1. \quad (\text{A1})$$

Calculating  $\mathbf{P}(t)$  up to  $(2N+1)$ th order we therefore get

$$\sum_{j=0}^N 4(2j+1) = (2N+2)^2 \quad (\text{A2})$$

contributions  $P_{n,m}(t)$  in Eq. (3.7), which can be discriminated by the computational procedure discussed in section III.C.

(ii) According to Eq. (3.9b)

$$\begin{aligned} \mathbf{P}^{(2N+1)}(t) = 2 \operatorname{Re} \sum_{j=0}^N \langle \Psi^{2(N-j)}(t) | \psi_0 \rangle \boldsymbol{\mu}_{01} \\ \times \langle \psi_1 | \Psi^{(2j+1)}(t) \rangle, \end{aligned} \quad (\text{A3})$$

the  $2N+1$  field-matter interactions contained in Eq. (A3) can be interpreted as  $2j+1$  interactions in the ket vector and  $2(N-j)$  interactions in the bra vector. Employing the RWA, the  $2j+1$  ket interactions can be identified as  $j+1$  absorption and  $j$  emission processes, while the  $2(N-j)$  bra interactions are identified as  $N-j$  absorption and  $N-j$  emission processes. By convention, absorption and emission processes in the ket vector yield the phase factor  $e^{i\mathbf{k}_i\mathbf{x}}$  and  $e^{-i\mathbf{k}_i\mathbf{x}}$ , respectively, while the corresponding bra interactions give the complex conjugate phase factors.

Let  $a_{\text{ket}}, 0 \leq a_{\text{ket}} \leq j+1$  ( $e_{\text{ket}}, 0 \leq e_{\text{ket}} \leq j$ ) be the number of absorption (emission) processes of field  $\mathbf{E}_1$  in the ket vector. As a consequence, we obtain  $j+1-a_{\text{ket}}$  ( $j-e_{\text{ket}}$ ) absorption (emission) processes in the field  $\mathbf{E}_2$ , yielding the phase factor of the ket vector

$$\exp\{i(e_{\text{ket}}-a_{\text{ket}})(\mathbf{k}_2\mathbf{x}-\mathbf{k}_1\mathbf{x})+i\mathbf{k}_2\mathbf{x}\}. \quad (\text{A4})$$

Analogously, let  $a_{\text{bra}}, 0 \leq a_{\text{bra}} \leq N-j$  ( $e_{\text{bra}}, 0 \leq e_{\text{bra}} \leq N-j$ ) be the number of absorption (emission) processes of field  $\mathbf{E}_1$  in the bra vector. We thus obtain  $N-j-a_{\text{bra}}$  ( $N-j-e_{\text{bra}}$ ) absorption (emission) processes in the field  $\mathbf{E}_2$ , yielding a bra phase factor of

$$\exp\{i(a_{\text{bra}}-e_{\text{bra}})(\mathbf{k}_2\mathbf{x}-\mathbf{k}_1\mathbf{x})\}. \quad (\text{A5})$$

The total phase factor acquired by the polarization  $\mathbf{P}^{(2N+1)}(t)$  is then given by

$$\exp\{i(e_{\text{ket}}-a_{\text{ket}}+a_{\text{bra}}-e_{\text{bra}})(\mathbf{k}_2\mathbf{x}-\mathbf{k}_1\mathbf{x})+i\mathbf{k}_2\mathbf{x}\}. \quad (\text{A6})$$

Since  $a_{\text{ket}}, e_{\text{ket}}, a_{\text{bra}}, e_{\text{bra}}$  are nonnegative and may vary independently, the highest prefactor of the phase difference  $(\mathbf{k}_2\mathbf{x}-\mathbf{k}_1\mathbf{x})$  is  $N$  (i.e., for  $a_{\text{ket}}=0, e_{\text{bra}}=0, e_{\text{ket}}=j, a_{\text{bra}}=N-j$ ), and the lowest prefactor is  $-(N+1)$  (i.e.,

for  $a_{\text{bra}}=0, e_{\text{ket}}=0, e_{\text{bra}}=N-j, a_{\text{ket}}=j+1$ ). Within the RWA, we therefore obtain  $2N+2$  directions of the polarization, i.e.

$$\mathbf{k} = n(\mathbf{k}_2 - \mathbf{k}_1) + \mathbf{k}_2, \quad n = -(N+1) \dots N \quad (\text{A7})$$

which is identical to Eq. (3.10).

(iii) Calculating the nonlinear polarization for nonoverlapping pulses within the RWA the following relations hold:

$$0 \leq a_{\text{ket}} - e_{\text{ket}} \leq 1, \quad (\text{A8a})$$

$$0 \leq a_{\text{bra}} - e_{\text{bra}} \leq 1, \quad (\text{A8b})$$

stating that the difference between the number of absorption and emission processes in the field  $\mathbf{E}_1$  is either 0 or 1 in the ket as well as in the bra vector. As a consequence, we obtain only three directions of the polarization, independent of the order of the perturbation expansion, with wave vectors

$$\mathbf{k} = n(\mathbf{k}_2 - \mathbf{k}_1) + \mathbf{k}_2, \quad n = -1, 0, 1. \quad (\text{A9})$$

## APPENDIX B

As has been discussed above, in the case of nonoverlapping pulses within the RWA we obtain coherent emission in the directions  $\mathbf{k}_1$  and  $2\mathbf{k}_2 - \mathbf{k}_1$ , while we obtain phase-insensitive emission in  $\mathbf{k}_2$  direction, which is due to stimulated emission and resonance Raman processes. In this appendix we wish to sketch a procedure which allows to discriminate the stimulated emission and stimulated Raman contributions. The general idea is most easily understood in the absence of vibronic coupling (i.e.,  $V_{01}=0$ ), i.e., we first assume that the two electronic states are exclusively coupled by the field-matter interaction  $H_{\text{int}}(t)$ .

When the pump and probe laser pulses do not overlap, it is possible to calculate the wave function of the system  $|\Psi(t)\rangle = \sum_{k=0,1} |\chi_k(t)\rangle |\psi_k\rangle$  at a time  $t$  that is after the action of the pump but before the action of the probe field. The main idea is to *independently* evaluate the overall polarization  $\mathbf{P}(t)$  for each electronic component  $|\chi_k(t)\rangle$  of  $|\Psi(t)\rangle$  (instead of evaluating  $\mathbf{P}(t)$  for the total wave function  $|\Psi(t)\rangle$ , cf. Eq. (3.6)). According to the definition of the two stimulated processes,<sup>24</sup> it is then clear that the action of the probe field on the ground-state component  $|\chi_0(t)\rangle$  yields the stimulated Raman contribution, while the action of the probe field on the excited-state component  $|\chi_1(t)\rangle$  yields the stimulated emission contribution. Furthermore it is easy to show that the “cross terms” that thus have been disregarded (i.e., the terms that involve both the ground and excited-state components) correspond to the coherent contributions which are emitted in directions  $\mathbf{k}_1$  and  $2\mathbf{k}_2 - \mathbf{k}_1$ . It should be stressed that the method described above does not involve perturbation theory in any step, i.e., the procedure applies as well to strong laser fields.

In the general case, transitions between the electronic states  $|\psi_0\rangle, |\psi_1\rangle$  may be caused by both the field-matter interaction  $H_{\text{int}}(t)$  and the intramolecular coupling  $V_{01}$ . Because the classification into “Raman emission” and “stimulated emission” solely refers to radiative transitions, we need to distinguish these two kinds of interaction in order to distinguish the types of emission. In the case at hand, this discrimination is possible as a consequence of a symmetry

property of the molecular Hamiltonian. Recall that the model system (3.3) consists of two electronic states  $|\psi_0\rangle, |\psi_1\rangle$  of different vibronic symmetry, which are coupled by the non-totally symmetric coupling mode  $Q_c$ . Hence the molecular Hamiltonian matrix decouples into two blocks, corresponding to the vibronic levels which transform according to the irreducible representations of  $\psi_0$  and  $\psi_1$ , respectively.<sup>50</sup> As a consequence, the two blocks of different vibronic symmetry may only couple through the field-matter interaction  $H_{\text{int}}(t)$ , but not through the vibronic interaction  $V_{01}$ . To discriminate the Raman and stimulated emission contributions, one may therefore proceed in complete analogy to the method described above, and evaluate the overall polarization *independently for each vibronic symmetry component* of the wave function. Note that the reasoning given above explicitly exploits the fact that in the model system (3.3) the two electronic states  $|\psi_0\rangle, |\psi_1\rangle$  are of different symmetry, i.e., the trick does not apply for coupled systems with electronic states of the same symmetry.

<sup>1</sup> *Femtochemistry*, Special Issue, edited by J. Manz and A. W. Castleman, Jr., J. Phys. Chem. **97** (1993); A. H. Zewail, *Femtochemistry—Ultrafast Dynamics of the Chemical Bond* (World Scientific, Singapore, 1994).

<sup>2</sup> *Ultrafast Phenomena IX*, edited by P. F. Barbara, W. H. Knox, G. A. Mourou, and A. H. Zewail (Springer, Heidelberg, 1994).

<sup>3</sup> L. R. Khundkar and A. H. Zewail, Annu. Rev. Phys. Chem. **41**, 15, (1990).

<sup>4</sup> J. M. Wiesenfeld and B. I. Greene, Phys. Rev. Lett. **51**, 1745 (1983).

<sup>5</sup> T. Baumert, B. Bühler, R. Thalweiser, and G. Gerber, Phys. Rev. Lett. **64**, 733 (1990).

<sup>6</sup> M. J. Rosker, F. W. Wise, and C. L. Tang, Phys. Rev. Lett. **57**, 321 (1986).

<sup>7</sup> H. L. Fragnito, J. Y. Bigot, P. C. Becker, and C. V. Shank, Chem. Phys. Lett. **160**, 101 (1989).

<sup>8</sup> J. Chesnoy and A. Mokhtari, Phys. Rev. A **38**, 3566 (1988).

<sup>9</sup> M. Mitsunaga and C. L. Tang, Phys. Rev. A **35**, 1720 (1987).

<sup>10</sup> G. Stock and W. Domcke, Chem. Phys. **124**, 227 (1988).

<sup>11</sup> W. T. Pollard, S.-Y. Lee, and R. A. Mathies, J. Chem. Phys. **92**, 4012 (1990).

<sup>12</sup> H. Metiu and V. Engel, J. Chem. Phys. **93**, 5693 (1990).

<sup>13</sup> Y. J. Yan and S. Mukamel, Phys. Rev. A **41**, 6485 (1990); S. Mukamel, Annu. Rev. Phys. Chem. **41**, 647 (1990); L. E. Fried and S. Mukamel, Adv. Chem. Phys. **84**, 435 (1993).

<sup>14</sup> S. H. Lin, B. Fain, and N. Hamer, Adv. Chem. Phys. **79**, 133 (1990).

<sup>15</sup> G. Stock and W. Domcke, Phys. Rev. A **45**, 3032 (1992).

<sup>16</sup> W. T. Pollard and R. A. Mathies, Annu. Rev. Phys. Chem. **43**, 497 (1992).

<sup>17</sup> M. Seel and W. Domcke, J. Chem. Phys. **95**, 7806 (1991).

<sup>18</sup> T. Baumert, V. Engel, C. Meier, and G. Gerber, Chem. Phys. Lett. **200**, 6410 (1992).

<sup>19</sup> A. D. Hammerich, R. Kosloff, and M. A. Ratner, J. Chem. Phys. **97**, 6410 (1992).

<sup>20</sup> M. Sugawara and Y. Fujimura, Chem. Phys. **175**, 323 (1993).

<sup>21</sup> L. Seidner, G. Stock, and W. Domcke, Chem. Phys. Lett. **228**, 665 (1994).

<sup>22</sup> G. Ebel and R. Schinke, J. Phys. Chem. **101**, 1865 (1994).

<sup>23</sup> U. Banin, A. Bartana, S. Ruhman, and R. Kosloff, J. Chem. Phys. **101**, 8461 (1994).

<sup>24</sup> Y. R. Shen, *The Principles of Nonlinear Optics* (Wiley, New York, 1984).

<sup>25</sup> M. Cho, N. F. Scherer, G. R. Fleming, and S. Mukamel, J. Chem. Phys. **96**, 5618 (1992).

<sup>26</sup> L. Seidner and W. Domcke, Chem. Phys. **186**, 27 (1994).

<sup>27</sup> A. Iosevici and W. E. Lamb, Phys. Rev. **185**, 517 (1969).

<sup>28</sup> J. H. Eberly and K. Wódkiewicz, J. Opt. Soc. Am. **67**, 1252 (1977).

<sup>29</sup> F. Bloch and A. Siegert, Phys. Rev. **57**, 522 (1940).

<sup>30</sup> R. Heather and H. Metiu, J. Chem. Phys. **90**, 6903 (1989).

<sup>31</sup> W. H. Hesselink and D. A. Wiersma, Chem. Phys. Lett. **56**, 227 (1978); J. Chem. Phys. **73**, 648 (1980).

<sup>32</sup> H. C. Longuet-Higgins, in *Advances of Spectroscopy*, edited by H. W. Thompson (Interscience, New York, 1961), Vol. 2, p. 429; F. T. Smith, Phys. Rev. **179**, 111 (1969).

<sup>33</sup> In the time-dependent formulation adopted here, “proportional to  $\mathbf{E}^n$ ” means  $\propto \int dt_n \dots \int dt_2 \int dt_1 \mathbf{E}(t_n) \dots \mathbf{E}(t_2) \mathbf{E}(t_1)$ .

<sup>34</sup> Several workers (e.g., Refs. 11, 13, 16, and 25) have used double-Feynman diagrams [T. K. Yee and T. K. Gustafson, Phys. Rev. A **18**, 1597 (1978)] or simplified versions of it to visualize nonlinear spectroscopic processes.

<sup>35</sup> G. Stock and W. Domcke, J. Opt. Soc. Am. B **7**, 1970 (1990).

<sup>36</sup> H. A. Ferwerda, J. Terpstra, and D. A. Wiersma, J. Chem. Phys. **91**, 3296 (1989).

<sup>37</sup> J. Michl and V. Bonačić-Koutecký, *Electronic Aspects of Organic Photochemistry* (Wiley, New York, 1990).

<sup>38</sup> W. M. Gelbart, K. F. Freed, and S. A. Rice, J. Chem. Phys. **52**, 2460 (1970).

<sup>39</sup> B. Bagchi, G. R. Fleming, and D. W. Oxtoby, J. Chem. Phys. **78**, 7375 (1983); B. Bagchi and G. R. Fleming, J. Phys. Chem. **94**, 9 (1990).

<sup>40</sup> A. Warshel, Z. T. Chu, and J.-K. Hwang, Chem. Phys. **158**, 303 (1991).

<sup>41</sup> G. J. M. Dormans, G. C. Groenenboom, and H. M. Buck, J. Chem. Phys. **86**, 4895 (1987).

<sup>42</sup> M. Persico, J. Am. Chem. Soc. **102**, 7839 (1980).

<sup>43</sup> C. Petrongolo, R. J. Buenker, and S. D. Peyerimhoff, J. Chem. Phys. **76**, 3655 (1982).

<sup>44</sup> G. Stock, L. Seidner, and W. Domcke, in Ref. 2, p. 512.

<sup>45</sup> G. Stock, R. Schneider, and W. Domcke, J. Chem. Phys. **90**, 7184 (1989).

<sup>46</sup> R. Schneider, W. Domcke, and H. Köppel, J. Chem. Phys. **92**, 1045 (1990).

<sup>47</sup> G. Stock, J. Chem. Phys. **101**, 246 (1994).

<sup>48</sup> U. Manthe and H. Köppel, J. Chem. Phys. **93**, 345, 1658 (1990).

<sup>49</sup> H.-D. Meyer and H. Köppel, J. Chem. Phys. **81**, 2605 (1984).

<sup>50</sup> H. Köppel, W. Domcke, and L. S. Cederbaum, Adv. Chem. Phys. **57**, 59 (1984).

<sup>51</sup> R. W. Schoenlein, L. A. Peteanu, R. A. Mathies, and C. V. Shank, Science **254**, 412 (1991); L. A. Peteanu, R. W. Schoenlein, R. A. Mathies, and C. V. Shank, Proc. Natl. Acad. Sci. USA **90**, 11762 (1993); Q. Wang, R. W. Schoenlein, L. A. Peteanu, S. J. Rosenthal, R. A. Mathies, and C. V. Shank, in Ref. 2, p. 425.

<sup>52</sup> G. Stock and W. H. Miller, Chem. Phys. Lett. **197**, 396 (1992); J. Chem. Phys. **99**, 1545 (1993).